

# Production and characterization of monoclonal anti-sphingosine-1-phosphate antibodies<sup>1</sup>

Nicole O'Brien,<sup>\*,†</sup> S. Tarran Jones,<sup>§</sup> David G. Williams,<sup>§</sup> H. Brad Cunningham,<sup>\*</sup> Kelli Moreno,<sup>\*</sup> Barbara Visentin,<sup>\*,†</sup> Angela Gentile,<sup>\*</sup> John Vekich,<sup>\*,†</sup> William Shestowsky,<sup>\*</sup> Masao Hiraiwa,<sup>\*</sup> Rosalia Matteo,<sup>\*</sup> Amy Cavalli,<sup>\*</sup> Douglas Grotjahn,<sup>\*\*</sup> Maria Grant,<sup>††</sup> Geneviève Hansen,<sup>\*</sup> Mary-Ann Campbell,<sup>\*</sup> and Roger Sabbadini<sup>2,\*,†</sup>

Lpath Inc.,<sup>\*</sup> San Diego, CA 92121; Department of Biology,<sup>†</sup> and Department of Chemistry and Biochemistry,<sup>\*\*</sup> San Diego State University, San Diego, CA 92182; MRC Technology,<sup>§</sup> London NW7 1AD, United Kingdom; and University of Florida,<sup>††</sup> Gainesville, FL

**Abstract** Sphingosine-1-phosphate (S1P) is a pleiotropic bioactive lipid involved in multiple physiological processes. Importantly, dysregulated S1P levels are associated with several pathologies, including cardiovascular and inflammatory diseases and cancer. This report describes the successful production and characterization of a murine monoclonal antibody, LT1002, directed against S1P, using novel immunization and screening methods applied to bioactive lipids. We also report the successful generation of LT1009, the humanized variant of LT1002, for potential clinical use. Both LT1002 and LT1009 have high affinity and specificity for S1P and do not cross-react with structurally related lipids. Using an *in vitro* bioassay, LT1002 and LT1009 were effective in blocking S1P-mediated release of the pro-angiogenic and prometastatic cytokine, interleukin-8, from human ovarian carcinoma cells, showing that both antibodies can out-compete S1P receptors in binding to S1P. *In vivo* anti-angiogenic activity of all antibody variants was demonstrated using the murine choroidal neovascularization model. Importantly, intravenous administration of the antibodies showed a marked effect on lymphocyte trafficking. The resulting lead candidate, LT1009, has been formulated for Phase 1 clinical trials in cancer and age-related macular degeneration. **■** The anti-S1P antibody shows promise as a novel, first-in-class therapeutic acting as a “molecular sponge” to selectively deplete S1P from blood and other compartments where pathological S1P levels have been implicated in disease progression or in disorders where immune modulation may be beneficial.—O'Brien, N., S. T. Jones, D. G. Williams, H. B. Cunningham, K. Moreno, B. Visentin, A. Gentile, J. Vekich, W. Shestowsky, M. Hiraiwa, R. Matteo, A. Cavalli, D. Grotjahn, M. Grant, G. Hansen, M-A. Campbell, and R. Sabbadini. **Production and characterization of monoclonal anti-sphingosine-1-phosphate antibodies.** *J. Lipid Res.* 2009. 50: 2245–2257.

*This work was supported in part by a grant from the National Cancer Institute (R44CA110298-3). Its contents are solely the responsibility of the authors and do not necessarily represent the official views of the National Cancer Institute or the National Institutes of Health.*

*Manuscript received 4 February 2009 and in revised form 22 May 2009.*

*Published, JLR Papers in Press, June 9, 2009  
DOI 10.1194/jlr.M900048-JLR200*

Copyright © 2009 by the American Society for Biochemistry and Molecular Biology, Inc.

This article is available online at <http://www.jlr.org>

**Supplementary key words** sphingosine-1-phosphate • monoclonal antibodies • angiogenesis • cancer • bioactive lipids • humanization • age-related macular degeneration • choroidal neovascularization • complementarity determining region • lymphocyte trafficking

Sphingosine-1-phosphate (S1P) is a bioactive lysophospholipid signaling molecule that serves important roles in normal development and physiological processes, including modulating the immune, cardiovascular, and central nervous systems (1–4). S1P is a key player in the sphingosine-1-phosphate signaling cascade and is produced from ceramide (CER) and sphingosine (SPH) through the action of sphingosine kinase (SPHK). While CER and SPH are intracellular promoters of apoptosis, S1P has opposite action and, in general, protects cells from apoptotic stimuli. Several experimental findings from independent research groups implicate S1P as a key mediator of multiple survival and growth-promoting pathways (5). The extracellular functions of S1P are initiated by the binding of the bioactive lipid to a set of five G protein-coupled receptors (GPCRs) belonging to the S1P receptor family (6). The balance between CER/SPH levels versus S1P provides a rheostat that determines whether a cell is sent into the death

Abbreviations: AMD, age-related macular degeneration; ATCC, American Type Culture Collections; CDR, complementarity determining region; CER, ceramide; CNV, choroidal neovascularization; EDC, 1-ethyl-3-[3-dimethylaminopropyl] carbodiimide hydrochloride; FR, framework region; GPCR, G protein-coupled receptor; IL-8, interleukin-8; IOA, iodoacetyl aminobenzoate; KLH, keyhole limpet hemocyanin; LPA, lysophosphatidic acid; mAb, monoclonal antibody; NHP, nonhuman primate; OD, optical density; S1P, sphingosine-1-phosphate; PS, phosphatidylserine; SMCC, sulfosuccinimidyl 4-[N-maleimidomethyl] cyclohexane-1-carboxylate crosslinker; SPH, sphingosine; SPHK, sphingosine kinase; SPR, surface plasmon resonance; sulfo-MBS, m-maleimidobenzoyl-N-hydroxysulfosuccinimide ester.

<sup>1</sup> Guest Editor for this article was Trudy Forte, Children's Hospital Oakland Research Institute (CHORI), Oakland, CA.

<sup>2</sup> To whom correspondence should be addressed.  
e-mail: rsabbadini@lpath.com

pathway or, alternatively, is protected from apoptosis (7–9). The key regulator of this rheostat is the kinase, SPHK1, which produces SIP for export and for autocrine and paracrine functions mediated by the cognate SIP receptors expressed on the surfaces of cancer, endothelial, and other cells. Interestingly, several types of human cancers exhibit increased expression of SPHK1 (10, 11) with a consequent dysregulation of SIP production and tumor progression (12, 13).

We postulate that effective treatment of these types of cancer necessitates a return to the appropriate balance of sphingolipid levels. This therapeutic strategy would deprive tumors of the growth promoter, SIP, and favor levels of the pro-apoptotic sphingolipids, SPH and CER. Fortunately, several intervention points exist for a sphingolipid-based therapeutic that allows for regulation of the rheostat. Most of these intervention points are protein targets, typically enzymes involved in the sphingolipid signaling cascade, the most prominent of which is SPHK1. Ideally, small molecule inhibitors of this enzyme would not only prevent the production of SIP but also shift the sphingolipid balance in favor of CER and SPH creating an opposing and balancing rheostat effect that could mitigate pathophysiological conditions induced by elevated SIP levels (14). However, small molecules demonstrate many pharmacokinetic, distribution, and toxicology problems that must be overcome before their therapeutic utility is established. Alternatively, the SIP receptors are considered to be points of potential therapeutic intervention (6) with small molecules, such as the SIP analog, FTY720 (Fingolimod), which is in clinical trials for multiple sclerosis (15, 16). However, this approach is complicated by the existence of at least five SIP-specific receptors that have overlapping functions and are differentially expressed by cells and organs.

One innovative approach for the treatment of cancer and other diseases includes the systemic administration of monoclonal antibodies (mAbs) to act as “molecular sponges” to neutralize extracellular tumor-promoting growth factors or cytokines, thus effectively lowering their bioavailability. Two such examples currently in use are: bevacizumab (Avastin<sup>®</sup>), which absorbs the pro-angiogenic growth factor, vascular endothelial growth factor; and adalimumab (Humira<sup>®</sup>) or infliximab (Remicade<sup>®</sup>), which neutralize the pro-inflammatory cytokine, tumor necrosis factor- $\alpha$ . We hypothesize that in diseases associated with SIP upregulation such as cancer, an anti-SIP antibody molecular sponge could lower the bioavailable SIP in the extracellular space to prevent ligand occupancy of, and signaling by, SIP receptors expressed on the target cancer cells.

The production of an antibody directed against a small (<400 Da) lipid such as SIP is a difficult and complex process. To date, there have been few successful attempts to produce functional antibodies to bioactive lipids with the high affinity and specificity necessary for diagnostic and therapeutic uses. In this report, we describe a method for the generation of antibodies against small bioactive lipids, such as SIP, a technology that employs thiolated lipid ana-

logs as a key component of the hapten used for both the immunization step and the antibody detection and potency assays. We generated, isolated, and characterized the first monoclonal IgG (LT1002) directed against bioactive SIP. This murine antibody also forms the basis of an ELISA that shows utility as a research tool to measure SIP in biological samples such as blood. We report here that LT1002 has been successfully humanized and optimized by complementarity determining region (CDR) grafting supported by intelligent design framework mutagenesis. This humanized version, LT1009, is a therapeutic candidate for treatment of patients with cancer or ocular diseases. Moreover, we show that both LT1002 and LT1009 can block the SIP-mediated release of interleukin-8 (IL-8) from human ovarian cancer cells (SKOV3) and that both demonstrate robust anti-angiogenic activity in the choroidal neovascularization (CNV) model of age-related macular degeneration (AMD) as well as disruption of lymphocyte trafficking when given intravenously. Together with other efficacy data previously published (17, 18), our results support the use of the humanized version of the anti-SIP mAb for Phase I trials in cancer and AMD.

## MATERIALS AND METHODS

### Materials

All lipids described in this report were obtained from Avanti Polar Lipids (Alabaster, AL; for lipid nomenclature, see footnotes and Table 3). Fatty acid esters were obtained from Sigma-Aldrich (St. Louis, MO). Normal mouse and human sera were obtained from Equitech-Bio (Kerrville, TX) and Golden West Biologicals (Temecula, CA), respectively. Succinimidyl-4-(*N*-maleimidomethyl) cyclohexane-1-carboxylate (SMCC), *N*-hydroxysulfosuccinimide, 1-ethyl-3-[3-dimethylaminopropyl] carbodiimide hydrochloride (EDC), and *m*-maleimidobenzoyl-*N*-hydroxysulfosuccinimide ester (sulfo-MBS) were purchased from Pierce Chemicals (Rockford, IL). A murine anti-SIP IgM (catalog no. 274042034) was obtained from Cosmo Bio Co. (Tokyo, Japan), and an isotype-matched nonspecific murine antibody (NS Ab) was purchased from Strategic Biosolutions (Newark, DE). A nonspecific human antibody was purchased from Jackson ImmunoResearch (West Grove, PA). Tumor cell lines were obtained from the American Type Culture Collections (ATCC; Rockville, MD). RPMI 1640 and  $\alpha$  MEM media were obtained by Invitrogen (Carlsbad, CA). McCoy's 5a medium with L-glutamine, penicillin/streptomycin, sodium bicarbonate, PBS without calcium and magnesium (1 $\times$  PBS), and 0.25% trypsin/EDTA solutions were purchased from Mediatech (Manassas, VA). FBS was obtained from multiple sources (Invitrogen, Mediatech, and Hyclone). Fatty-acid-free BSA was purchased from Calbiochem (San Diego, CA). The mouse monoclonal antibody isotyping kit (IsoStrip) was obtained from Roche Applied Science (Indianapolis, IN).

### Synthesis of sphingolipid analogs and conjugates

An analog to *D*-erythro-SIP was synthesized to contain a sulfhydryl group on the C18 terminal carbon of the hydrocarbon chain capable of cross-linking to either protein carriers or to the Biacore chip. Organic synthesis of the thiolated derivatives is described elsewhere (D. Grotjahn, unpublished observations). For immunization, the thiolated SIP analog was conjugated to keyhole limpet hemocyanin (KLH) or to fatty-acid-free BSA via SMCC (Pierce/Thermo Fisher Scientific) using protocols recom-

mended by the manufacturer. SMCC is a heterobifunctional cross-linker that reacts with primary amines and sulfhydryl groups to form stable amide and thioether bonds. Thiolated SIP (50  $\mu$ l, 25 mg/ml in DMSO) was combined with SMCC-activated KLH or BSA (400  $\mu$ l, 10 mg/ml in PBS) and incubated for 2 h at room temperature. The reaction mixture was then applied to a protein-desalting spin column (Pierce, Thermo Fisher Scientific) equilibrated with PBS to obtain lipid-SMCC-BSA conjugate. Alternatively, the thiolated SIP was coupled to KLH via an iodoacetyl aminobenzoate (IOA) linker. For this conjugation, the IOA spacer was introduced to fatty-acid-free BSA using *N*-sulfo-succinimidyl [4-iodoacetyl] aminobenzoate. Fatty-acid-free BSA (250  $\mu$ l, 10 mg/ml) and *N*-sulfo-succinimidyl [4-iodoacetyl] aminobenzoate (25  $\mu$ l, 7 mg/ml) were combined and incubated for 30 min at room temperature. The thiolated lipid (30  $\mu$ l, 25 mg/ml in DMSO) was combined with the purified IOA-BSA (240  $\mu$ l, 8–9 mg/ml) and incubated for 1 h at room temperature. The resulting lipid-IOA-BSA conjugate was purified using protein desalting spin column as described. The protein concentration was adjusted to 2 mg/ml based on A280 determination using BSA and KLH as standard.

### Murine antibody production

Briefly, Swiss Webster or BALB/c mice were immunized four times over a 2 month period with 50  $\mu$ g of SIP-SMCC-KLH with Freund's adjuvant. Immunization was performed at Strategic Bio-Solutions (Newark, DE) under a protocol approved by the Institutional Animal Care and Use. SIP-IOA-KLH or SIP-IOA-BSA immunogens were also tested as immunogens. Serum samples were collected 2 weeks after the second, third, and fourth immunizations and screened by direct ELISA for anti-SIP antibody (see below). Of the 55 mice immunized, eight animals showed significant serum titers of antibodies to SIP. Spleens from mice that displayed high antibody titers were subsequently used to generate hybridomas using standard spleen cell/myeloma fusion and selection procedures. The resulting monoclonal hybridomas were grown to confluency and the cell supernatants collected for ELISA analysis. One hybridoma performing especially well (clone 306D326.26) was deposited with the ATCC (safety deposit storage number SD-5362) and represents the first murine IgG directed against SIP (referred to as LT1002 or *Sphingomab*<sup>TM</sup>). The clone contains the CDRs used to generate humanized antibody LT1009 (*Sonepizumab*<sup>TM</sup>).

For production of LT1002 as ascites (125 ml), 50 severe combined immune deficiency mice were injected intraperitoneally with the LT1002 clone. LT1002 was purified by Protein A affinity chromatography, yielding 429 mg of IgG. Endotoxin contamination was <3 EU/mg in tests performed by Cambrex (East Rutherford, NJ). LT1002 was determined to be IgG kappa1 isotype using the Roche IsoStrip kit and >95% pure by analytical HPLC. Purified antibody was dialyzed into 20 mM sodium phosphate, 150 mM sodium chloride at pH 7.2 and stored at -70°C.

### Design of the humanization of the anti-SIP mAb

LT1002 was humanized by grafting the mouse CDRs into human framework regions (FRs) (19, 20). The Kabat definition of CDRs was used (21, 22). Human FR sequences were selected from the International Immunogenetics and Kabat databases based on sequence identity with LT1002 and using the sequence analysis program SR v7.6 (supplied by Steve Searle; Wellcome Trust Sanger Institute, Cambridge, UK). Sequences with high identity at vernier (23), canonical (20), and V<sub>H</sub>-V<sub>L</sub> interface (22) residues were selected. Human FRs with fewest nonconservative differences at these positions, and with matching CDR lengths (except CDR H3), were considered for use in humanization.

Human V<sub>L</sub> and V<sub>H</sub> sequences, AY050707 and AJ002773, respectively, were selected as acceptor FRs for the mouse LT1002 CDRs. As a result of expression and antigen binding analysis of a number of variant V<sub>H</sub> sequences, FR residues 2, 27, 37, 48, 67, and 69 were substituted with the equivalent residues in LT1002. Similarly, V<sub>L</sub> FR positions, 4, 36, 49, 64, and 67 were replaced with the equivalent residues in LT1002. In addition, a C residue located in CDR2 of the heavy chain was substituted with A, G, S, or F in an effort to protect the humanized variants from C oxidation. The mutation to A was chosen for further studies. These variants were expressed, as whole IgG, together with the humanized light chain containing either three or five back mutations. All the lead humanized variants were compared by BiaCore affinity analysis, by antigen binding specificity and potency by ELISA, and by antigen binding stability to elevated temperature challenge.

### Generation of the humanized antibody variants

The heavy and light chain variable regions of LT1002 were cloned and expressed as a whole chimeric IgG<sub>1</sub>K antibody. The antigen binding potency of this chimeric antibody validated the determined DNA sequences of LT1002. Subsequently, the Kabat CDRs (1, 2, and 3,) from LT1002 V<sub>H</sub> and V<sub>L</sub> were grafted into the acceptor frameworks of AJ002773 and AY050707, respectively. **Table 1** defines the numerical descriptions for the various antibody forms. The humanized variants were transiently expressed in HEK 293 cells in serum-free conditions, their antigen binding potency was measured by ELISA, and their affinity was analyzed by BiaCore.

### Mouse antibody cloning, mutagenesis, and antibody expression and purification

Anti-SIP hybridomas were grown in DMEM (with GlutaMAX<sup>TM</sup> I), adjusted to contain 4.5 g/L D-glucose, sodium pyruvate, 1 $\times$  glutamine/penicillin/streptomycin (Gibco/Invitrogen, Carlsbad, CA), and 10% FBS (Fetal Clone I; Perbio Science/Thermo Scientific). Total RNA was isolated from 10<sup>7</sup> hybridoma cells using a procedure based on the RNeasy Mini kit (Qiagen, Valencia, CA). Total RNA was used to generate first-strand cDNA following the manufacturer's protocol (first-strand synthesis kit from Amersham Biosciences, Piscataway, NJ).

The mouse immunoglobulin heavy chain variable region (VH) cDNA was amplified by PCR using the MHV7 primer (MHV7; 5'-ATGGRATGGAGCKGGRTCTTTMTCTT-3') in combination with mouse constant region primers MHCG1/2a/2b/3 (MHCG1, 5'-CAGTGGATAGACAGATGGGGG-3'; MHCG2a, 5'-CAGTGGATAGACCGATGGGGC-3'; MHCG2b, 5'-CAGTGGATAGACTGATGGGGG-3'; MHCG3, 5'-CAAGGGATAGACAGATGGGGC-3'). The product of the reaction was ligated into the pCR2.1<sup>®</sup>-TOPO<sup>®</sup> vector using the TOPO-TA cloning<sup>®</sup> kit and sequenced. The variable domain of the heavy chain was then amplified by PCR from this vector and inserted as a *HindIII*/*Apal* fragment and ligated into the expression vector, pG1D200, which contains HCMVi promoter, a leader sequence and the  $\gamma$ -1 constant region. This generated plasmid pG1D200306DVH.

Similarly, the mouse immunoglobulin kappa chain variable region (VL) was amplified by PCR using the VK20 (5'-GTCTCTGATTCTAGGGCA-3') primer in combination with the kappa constant region primer MKC (5'-ACTGGATGGTGGGAA-GATGG-3'). The product of the reaction was ligated into the pCR2.1<sup>®</sup>-TOPO<sup>®</sup> vector using the TOPO-TA cloning<sup>®</sup> kit and sequenced. The variable domain of the light chain was amplified by PCR and inserted as a *BamHI*/*HindIII* fragment into the expression vector pKN100, which contains HCMVi promoter, a leader sequence and the human kappa constant domain. This generated pKN100306DVK.



TABLE 1. Antibody designation and binding affinity

| Designation | mAb | Mutations  |                             | K <sub>a</sub> (M <sup>-1</sup> s <sup>-1</sup> ) | K <sub>d</sub> (s <sup>-1</sup> ) | K <sub>d</sub> (nM) |
|-------------|-----|------------|-----------------------------|---|-----------------------------------|---------------------|
|             |     | HC         | LC                          |   |                                   |                     |
| LT1002      | M   | –          | –                           | 1.18 ± 7 × 10 <sup>7</sup>                        | 3.10 ± 1 × 10 <sup>-4</sup>       | 0.03 ± 0.002        |
| LT1003      | C   | –          | –                           |   |                                   |                     |
| LT1004      | Hu  | V37M       | Y49S, G64S, S67Y            | 1.95 ± 2 × 10 <sup>5</sup>                        | 2.09 ± 9 × 10 <sup>-4</sup>       | 1.06 ± 0.010        |
| LT1006      | Hu  | V37M       | L4V, Y36F, Y49S, G64S, S67Y | 8.48 ± 9 × 10 <sup>4</sup>                        | 5.82 ± 8 × 10 <sup>-5</sup>       | 0.69 ± 0.010        |
| LT1007      | Hu  | V37M, C50A | Y49S, G64S, S67Y            | 2.16 ± 1 × 10 <sup>7</sup>                        | 8.95 ± 8 × 10 <sup>-4</sup>       | 0.04 ± 0.004        |
| LT1009      | Hu  | V37M, C50A | L4V, Y36F, Y49S, G64S, S67Y | 8.23 ± 4 × 10 <sup>6</sup>                        | 4.82 ± 3 × 10 <sup>-4</sup>       | 0.06 ± 0.005        |

M, mouse; C, chimeric; Hu: humanized. K<sub>a</sub> = Association rate constant in M<sup>-1</sup> s<sup>-1</sup>. K<sub>d</sub> = Dissociation rate constant in s<sup>-1</sup>. K<sub>d</sub> = k<sub>d</sub>/k<sub>a</sub> Dissociation rate constant.

Mutations within the variable domain sequences were created using the QuikChange site-directed mutagenesis kit (Stratagene, CA). Individual reactions were carried out with 50 ng of double-stranded DNA template, 2.5 U of *PfuUltra HF DNA* polymerase and its corresponding buffer, 10 mM deoxynucleoside triphosphate mix, and 125 ng of each of the mutagenic oligonucleotides resuspended in 5 mM Tris-HCl (pH 8.0) and 0.1 mM EDTA. The initial denaturation was carried out at 95°C for 30 s, followed by 16 cycles of amplification: 95°C for 30 s, 55°C for 60 s, and 68°C for 8 min. The reaction product was digested with *DpnI* at 37°C for 1 h to remove methylated parental DNA. The resultant mutant was transformed into competent XL1-Blue *Escherichia coli* and plated on LB-agar containing 50 µg/ml ampicillin. The colonies were then checked by sequencing. Each of the mutants was then cultured in 1 liter flasks and purified using the EndoFree Plasmid Purification Kit (Qiagen).

The heavy- and light-chain plasmids were transformed into Top 10 *E. coli* (One Shot Top 10 chemically competent *E. coli* cells; Invitrogen) and stored in glycerol. Large-scale plasmid DNA was prepared as described by the manufacturer (endotoxin-free MAXIPREP™ kit; Qiagen). Plasmids were transfected into the human embryonic kidney cell line 293F using 293fectin and 293F-FreeStyle Media for culture. Light- and heavy-chain plasmids were both transfected at 0.5 µg/ml following the manufacturer's instructions. The yield was approximately 10–20 mg/l IgG for the humanized variants (LT1004, LT1006, and LT1007) and 0.3–0.5 mg/ml IgG for LT1003. SDS-PAGE under reducing conditions revealed two bands at 25 and 50 kDa with high purity (>98%), consistent with the mass of immunoglobulin light and heavy chains, respectively. A single band was observed under nonreducing conditions with the expected mass of ~150 kDa.

Monoclonal antibodies were purified from culture supernatants by passing culture supernatants through protein A/G columns (Pierce, Thermo Fisher Scientific) at 1.0 ml/min. Mobile phases consisted of 1× Pierce IgG binding buffer and 0.1 M glycine, pH 2.7. Antibody eluted in 0.1 M glycine was diluted with 0.1 volumes of 1 M phosphate buffer, pH 8.0, to neutralize the pH, and then pooled and dialyzed (Pierce Slide-A-Lyzer Cassette, 3500 MWCO) against PBS. Elutes were concentrated using Centricon YM-3 (10,000 MWCO; Amicon/Millipore, Jaffrey, NH) by centrifugation for 1 h at 2,500 g. The antibody concentration was determined by quantitative ELISA (below) using a commercial myeloma IgG<sub>1</sub> stock solution as a standard. Testing for endotoxin (Cambrex/Lonza, Allendale, NJ) of batches for in vivo work indicated levels <3 EU/mg.

#### Quantitative ELISA for protein determination

ELISA plates (Corning Costar, Clovis, CA) were coated with rabbit anti-mouse IgG F(ab')<sub>2</sub> (catalog no. 315-006-047; Jackson ImmunoResearch) or rabbit anti-human, IgG F(ab')<sub>2</sub> (catalog no. 309-006-006) diluted in 0.1 M carbonate buffer (100 mM NaHCO<sub>3</sub> and 33.6 mM Na<sub>2</sub>CO<sub>3</sub>, pH 9.5) at 37°C for 1 h. Plates

were washed with PBS and blocked with PBS/BSA/Tween 20 for 1 h at 37°C. For the primary incubation, serial dilutions (100 µl/well) of nonspecific mouse or human IgG (used for the calibration curve) and samples to be measured were added to the wells. Plates were washed and incubated with 100 µl/well of HRP-conjugated goat anti-mouse IgG (catalog no. 115-035-146; Jackson ImmunoResearch) diluted 1:40,000 or HRP-conjugated goat anti-human (catalog no. 109-035-003) diluted 1:50,000 for 1 h at 37°C. After washing, the enzymatic reaction was developed with tetramethylbenzidine (Sigma-Aldrich) and stopped by adding 1 M H<sub>2</sub>SO<sub>4</sub>. The optical density (OD) was measured at 450 nm using a Thermo Multiskan EX. Raw data were transferred to GraphPad software for analysis.

#### Direct ELISA

ELISA plates (Corning Costar; Lowell, MA) were coated with S1P-SMCC-BSA diluted in 0.1 M carbonate buffer (pH 9.5) at 37°C for 1 h. Plates were washed with PBS (137 mM NaCl, 2.68 mM KCl, 10.1 mM Na<sub>2</sub>HPO<sub>4</sub>, and 1.76 mM KH<sub>2</sub>PO<sub>4</sub>, pH 7.4) and blocked with 1% BSA in PBS containing 0.1% Tween 20 for 1 h at room temperature or overnight at 4°C. For the primary incubation (1 h at room temperature), a dilution series of the anti-S1P mAbs produced from each hybridoma (0.4, 0.2, 0.1, 0.05, 0.0125, and 0 µg/ml) was added to the plate (100 µl/well). Plates were washed and incubated with HRP-conjugated goat anti-mouse IgG (1:20,000 dilution; catalog no. 115-035-003; Jackson ImmunoResearch) or HRP-conjugated goat anti-human IgG (catalog no. 109-035-003) diluted to 1:50,000 (100 µl/well) for 1 h at room temperature. After washing, the peroxidase chromogenic substrate, tetramethylbenzidine (Sigma-Aldrich) was added, and color development was stopped by adding 1 M H<sub>2</sub>SO<sub>4</sub>. OD values were measured at 450 nm using a Thermo Multiskan EX. Raw data were transferred to GraphPad software for analysis. For the direct ELISA using the anti-S1P IgM, the secondary antibody, HRP-conjugated F(ab')<sub>2</sub> goat anti-mouse IgG + IgM (catalog no. 115-036-068; Jackson ImmunoResearch) was used at 1:20,000 dilution.

#### Competition ELISA

The specificity of the anti-S1P mAbs was tested by competition ELISA. This assay is similar to the direct ELISA. However, the primary incubation contained 0.8 µg/ml of the various anti-S1P mAbs, mixed with one competitor lipid from the list: e.g., S1P, lysophosphatidic acid (LPA), phosphatidylserine (PS), PE, CER, C1P, SPH, DH-SPH, SM, SPC, and DH-S1P.

#### Antibody binding kinetics by surface plasmon resonance

All surface plasmon resonance (SPR) data were collected on a Biacore 2000 optical biosensor (Salt Lake City, UT). S1P was coupled to a maleimide-activated CM5 sensor chip. First, the CM5 chip was activated with an equal mixture of NHS/EDC for 7 min followed by a 7 min blocking step with ethylenediamine. Next,

sulfo-MBS (0.05 mM in HEPES-buffered saline, 10 mM HEPES, 150 mM NaCl, and 0.005% p20, pH 7.4; Pierce/Thermo Fisher Scientific) was passed over the chip. The S1P coating material (0.1 mM in HEPES-buffered saline) injected for two time periods, producing two S1P surface densities (305 and 470 total response units bound). Binding data were collected for a 3-fold dilution series of LT1002, LT1004, LT1006, LT1007, and LT1009 starting at 16.7, 50.0, 50.0, 16.7, and 16.7 nM, respectively. SPR binding at each concentration was tested twice. Surfaces were regenerated with 50 mM NaOH. All data were collected at 25°C. Response data were normalized to a reference, blocked surface and to blank injections. The data sets were curve-fitted to theoretical interaction models to obtain binding parameters. Data from the different concentrations used global fit to determine apparent binding rate constants. The number in parentheses indicates the error in the last digit. The calculated apparent affinity constants could reflect an avidity component of antibody binding.

### Thermostability measurements

Purified antibodies (25 µg/ml) were distributed into microtubes and incubated for 10 min in a PCR block at temperatures between 50 and 80°C, before rapid cooling to 4°C. These temperatures were chosen based on the denaturation profile observed for the murine antibody. Subsequently, the heated samples were tested for binding to S1P by direct ELISA as described above.

### CXCL8/IL-8 cytokine release from SKOV3 cells

Human ovarian carcinoma (SKOV3) cell line was purchased from ATCC and cultured in McCoy's 5a medium with 2.2 g/l L-glutamine and adjusted to contain 1% penicillin streptomycin solution, 2.2 g/l sodium bicarbonate, and 10% FBS (Hyclone; Thermo Fisher Scientific). Tumor cells were subcultured twice a week at 37°C in a 5% CO<sub>2</sub> humidified incubator. For the in vitro assay, SKOV3 cells did not exceed passage 12. SKOV3 cells were seeded in a 96-well plate at the density of  $1 \times 10^4$  cells per well. Tumor cells were then serum starved in minimum medium (McCoy's Media 5a, adjusted to contain 2.2g/l L-glutamine, 2.2 g/l sodium bicarbonate, and 1 mg/ml fatty-acid-free BSA) for exactly 24 h. After serum starvation, SKOV3 cells were treated with 5 µM S1P (solubilized in 4 mg/ml fatty-acid-free BSA in PBS) previously incubated in the presence or absence of various concentrations of either LT1009 or LT1002 (2–2,500 µg/ml antibody; 1 h at 37°C and 5% CO<sub>2</sub> humidified incubator). After 18 h, conditioned media were collected and tested by human IL-8 ELISA (Human CXCL8/IL-8 Quantikine Kit). IL-8 values (pg/ $1 \times 10^4$  cells) were calculated (GraphPad software) and expressed as the fold increase over untreated cells (NT). The IC<sub>50</sub> for LT1009 and LT1002 were calculated using a nonlinear fit of log dose versus response using a least square (ordinary) fitting method.

### Murine CNV model

CNV lesions were induced and quantified as previously described (24, 25), including the intravitreal injection of anti-S1P mAbs (18).

### Lymphocyte trafficking

A pharmacodynamic study designed to test the ability of LT1009 and LT1002 to alter lymphocyte trafficking in mice was performed at BioQuant (San Diego, CA). Adult male C57Bl/6J mice, five per treatment group, received single intravenous injections of LT1002, LT1009, control human IgG, or PBS. Total lymphocyte counts were performed on blood samples drawn before and after antibody treatment using an automated analyzer

(VetScan, Abaxis). Statistical analyses were performed using GraphPad Prism software.

### Animal use

All animal studies presented in this work were conducted in conformity with the Public Health Service Policy on Humane Care and Use of Laboratory Animal Research Guide for Care and Use of Laboratory Animals at Strategic BioSolutions, BioQuant, and the University of Florida.

## RESULTS

### Production of murine anti-S1P monoclonal antibodies

Immune responses in mice were initially generated using a thiolated D-erythro-S1P analog conjugated to either KLH or BSA carrier proteins. The thiolated S1P analog was specifically synthesized to possess a reactive sulfhydryl group at the terminal C18 carbon of the S1P hydrocarbon chain, rendering the lipid chain capable of being covalently linked to the protein carrier molecules via SMCC or IOA cross-linking agents. Thus, hapten-carrier conjugation was achieved without disturbing the epitope of interest, which is the polar head group of S1P. Using this protocol, multiple combinations of hapten, linker, and carrier are possible, for example, S1P-SMCC-KLH (or BSA) and S1P-IOA-KLC (or BSA; for details, see Materials and Methods). During immunization, mice responded favorably in generating high titer antibodies to the immunogen using either KLH or BSA protein carriers, and, interestingly, the responses were independent of which protein or chemical cross-linker was used to form the hapten (see below).

Screening of mouse serum and cell supernatants for S1P-specific antibodies was done by direct ELISA using the thiolated S1P analog conjugated to fatty-acid-free BSA (S1P-SMCC-BSA) as the coating material. Of the resulting 1,500 hybridomas, 287 positive hybridomas were identified, 159 of which showed significant titers. Each of the 159 hybridomas was further screened to obtain 60 stable, high titer hybridomas. After a further two rounds of re-screening, one lead hybridoma (306D326.26) was isolated that represents the first murine anti-S1P IgG (LT1002 or *Sphingomab*<sup>TM</sup>). **Figure 1A** shows a direct ELISA of purified anti-S1P mAb from the LT1002 using S1P-SMCC-BSA as the coating material. LT1002 was isotypized as IgG1-κ, and its performance characteristics were compared with a commercially available IgM antibody produced by immunizing mice with a liposomal complex containing S1P (anti-S1P IgM; CosmoBio Co., Japan). These data demonstrate that, by comparison with the commercial IgM antibody, LT1002 exhibited superior ability to recognize S1P in the direct ELISA. In many cases, immunization with bioactive lipids (e.g., CER) as emulsions, liposomal complexes, or in the presence of colloidal gold, has resulted in IgMs (26), which have limited utility with regard to specificity, sensitivity, and biological activity in comparison to IgG (27). IgMs form large aggregates that may limit their utility as reagents or therapeutics. In fact, all commercially available therapeutic antibodies are IgGs.

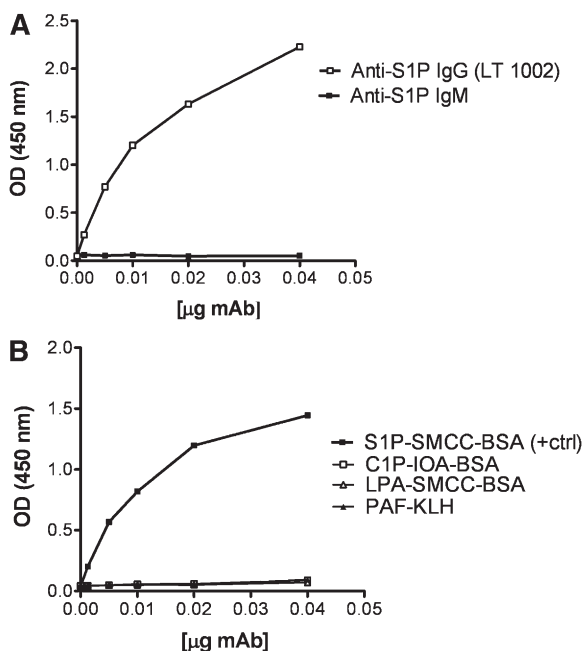


**Fig. 1.** A: Direct ELISA for measurement of the murine mAb, LT1002, binding to S1P. The S1P binding affinity of the murine mAb, LT1002, and a commercially available murine IgM antibody were compared by direct binding ELISA. Each antibody was measured at six concentrations ranging from 400–12.5 ng/ml on a 96-well plate coated with S1P-SMCC-BSA and detected using HRP-conjugated anti-mouse IgG and IgM secondary antibodies. The binding activity is expressed as OD at 450 nm. B: Direct ELISA for measurement of the murine mAb, LT1002, binding to S1P versus binding to cross-linker or carrier proteins. The specific binding of the murine mAb, LT1002, to S1P versus binding to cross-linkers IOA or SMCC and to carrier proteins KLH or BSA was assessed using a direct binding ELISA. LT1002 antibody was measured at six concentrations ranging from 400–12.5 ng/ml on a 96-well plate coated with S1P-SMCC-BSA (positive control), C1P-IOA-BSA, LPA-SMCC-BSA, and PAF-KLH. Primary antibody was then detected using HRP-conjugated anti-mouse IgG secondary antibody. The binding activity is expressed as OD at 450 nm.

The use of the S1P-SMCC-BSA conjugate as coating material in the direct ELISA was critical to the efficient selection of responder mice and in the quantitative screening of antibody-producing hybridomas. The use of this covalent conjugate was preferred over a simple noncovalent complex between S1P and fatty-acid-free BSA because washing steps in the ELISA would result in loss of noncovalently bound S1P. Critical control experiments were done to ensure that the antibodies did not recognize either the protein carrier or the cross-linker moiety. Figure 1B demonstrates that, even though LT1002 recognized S1P-SMCC-BSA, it did not recognize LPA-SMCC-BSA, suggesting that the murine mAb was not directed against LPA, SMCC, or BSA. Additionally, LT1002 did not recognize C1P-IOA-BSA, indicating that it did not bind to the cross-linker IOA or to C1P. The lack of binding to linker-free PAF-KLH indicated that LT1002 did not recognize the protein carrier KLH. Similar results were obtained using one of the humanized variant, LT1009 (data not shown).

As shown in Fig. 1B, LT1002 binds *D-erythro*-S1P but not CER or LPA. More importantly, the antibody also recog-

nizes the *D-erythro*-sphinganine-1-phosphate, the fully saturated form of S1P (Table 2), suggesting that the polar head group is a more important part of the epitope than is the hydrocarbon chain.

It is well accepted that most existing antibodies to phospholipids commonly recognize an oxidized form of the lipid rather than its natural unmodified structure (28, 29). For this reason, we wanted to determine if *D-erythro*-S1P was susceptible to oxidation under our laboratory conditions. This form of S1P has one double bond in the 4-5 carbon position and is generally not susceptible to oxidation damage. However, to confirm the specificity of our antibodies for unoxidized S1P, we performed reverse phase HPLC of the unsaturated and potentially oxidizable S1P variant *D-erythro*-S1P using methods reported previously (30). *D-erythro*-S1P was incubated for 48 h at room temperature in air, prior to HPLC analysis. The results showed no change in HPLC retention time after air incubation, suggesting that S1P is not easily oxidized, that S1P in our ELISA and SPR assays remains unoxidized, and therefore that LT1002 binds the unoxidized form of S1P (data not shown).

### Humanization and optimization of the anti-S1P mAb

Therapeutic use of a murine mAb in humans generally requires humanization to avoid a human anti-mouse antibody response that can reduce efficacy in patients as a consequence of the neutralization and rapid elimination of immune complexed antibody. For this reason, the murine antibody LT1002 was humanized.

Humanization of LT1002 was performed by grafting the six murine CDRs into the framework (FR) of human immunoglobulin light- and heavy-chain variable regions. Reversion by back mutation of selected residues in the human FR to the equivalent residues in LT1002 was necessary to obtain adequate affinity (data not shown). All antibody variants are described in Table 1. Humanization of LT1002  $V_H$  required only one murine FR back mutation to restore S1P binding activity, while three or five murine FR back mutations were necessary in  $V_L$  to achieve binding affinity equivalent to that found with LT1002.

Mutations at five key positions ( $V_L$ : Y49S, G64S, S67Y; and  $V_H$ : V37M and C50A) were found to influence S1P binding to support the position of the CDRs as they were presented by the murine framework. According to the homology model of mouse antibody LT1002, the  $V_L$  residues S64 and Y67 are in close proximity to CDR L2 and CDR L1, respectively, and S49 is positioned at approximately van der Waals distance from the side chains of R55 in CDR L2 and W107 in CDR H3.  $V_H$  residue M37 is proximal to the hydrophobic FR residues F98 ( $V_L$ ), L45 ( $V_H$ ), F95 ( $V_H$ ), and W111 ( $V_H$ ). Interestingly, the Y49S back mutation in  $V_L$  dramatically improved S1P binding affinity (data not shown). The main role of  $V_L$  S49 is to provide structural support to  $V_L$  R55 (CDR L2) and H3. The C50A CDR H2 mutation was introduced to remove an unpaired cysteine residue eliminating the potential for oxidative damage. Interestingly, this back mutation actually within the CDR improved the antigen binding potency. The effects of this particular back mutation as well as other back



TABLE 2. Specificity of LT1002 and LT1009 to lipid targets in competitive ELISA

| Common Name                    | Lipid Competitor<br>Nomenclature by Lipid Map                                       | Percentage of Inhibition at 2 $\mu$ M |                  |
|--------------------------------|---|---------------------------------------|------------------|
|                                |   | LT1002                                | LT1009           |
| S1P                            | Sphing-4-enine-1-phosphate  | 89.63 $\pm$ 2.74                      | 88.10 $\pm$ 0.32 |
| Dihydrosphingosine-1-phosphate | Octadecasphinganine-1-phosphate   | 49.20 $\pm$ 1.63                      | 73.20 $\pm$ 1.00 |
| D-erythro-sphingosine          | Sphing-4-enine  | NI                                    | 12.64 $\pm$ 2.59 |
| Dihydrosphingosine             | Octadecasphinganine   | 8.28 $\pm$ 0.35                       | 0.75 $\pm$ 2.23  |
| Sphingosyl phosphorylcholine   | Sphing-4-enine-1-phosphocholine   | 56.68 $\pm$ 0.43                      | 51.51 $\pm$ 2.05 |
| CER                            | N-(9Z-Octadecenoyl)-sphing-4-enine  | NI                                    | NI               |
| Ceramide-1-phosphate           | N-(Dodecyl)-sphing-4-enine-1-phosphate  | NI                                    | 2.49 $\pm$ 2.68  |
| Lysophosphatidic acid          | 1-(9Z-Octadecenoyl)-sn-glycerol-3-phosphate   | 2.13 $\pm$ 5.10                       | 7.80 $\pm$ 3.10  |
| Platelet activating factor     | 1-O-Hexadecyl-2-acetyl-sn-glycerol-3-phosphocholine                                 | NI                                    | NI               |
| Sphingomyelin                  | N-(9Z-Octadecenoyl)-sphing-4-enine-1-phosphocholine                                 | NI                                    | 16.12 $\pm$ 0.74 |
| Phosphatidylethanolamine       | 1-Octadecyl-2-(5Z, 8Z, 11Z, 14Z-eicosatetraenoyl)-sn-glycerol-3-phosphoethanolamine | NI                                    | 4.53 $\pm$ 0.88  |
| Phosphatidylserine             | 1,2-Bis-octadecyl-sn-glycerol-3-phosphoserine                                       | NI                                    | 4.83 $\pm$ 1.76  |
| Phosphatidic acid              | 1-Hexadecyl-2-(9Z-octadecenoyl)-sn-glycerol-3-phosphate                             | NI                                    | 0.92 $\pm$ 2.28  |
| Lysophosphatidylcholine        | 1-Octadecyl-sn-glycerol   | NI                                    | 3.92 $\pm$ 3.36  |
| Phosphatidylcholine            | 1-Hexadecyl-2-octadecyl-sn-glycerol-3-phosphocholine                                | NI                                    | NI               |

NI, no inhibition.

mutations in the framework are evident from crystal structure of the LT1009 Fab where specific interactions between the lipid and the antibody are elucidated at high resolution (30a).

#### Affinity and stability of the humanized antibody variants

The biophysical properties of several humanized variants were characterized for their binding affinity, potency, and stability. The binding kinetics of S1P to its receptors or other moieties has traditionally been problematic because of the insolubility of lipids in aqueous solutions. For BiaCore measurement of SPR, these problems were overcome by directly immobilizing the thiolated S1P to an activated CM5 BiaCore chip. The chip was coated with various densities of S1P (7, 20, and 1000 total RUs bound), and the antibody variants were injected into the flow cell. Antibody binding data were globally fitted to a bivalent interaction model. Comparative analysis of the model and sensograms (data not shown) validated the use of this model and gave confidence in the calculated S1P binding affinities. Table 1 presents the binding affinity of each humanized variant and compares the  $K_a$ ,  $K_d$ , and  $K_d$  with those of LT1002. Two variants, LT1004 and LT1006, exhibited binding affinities in the low nanomolar range similar to the chimeric anti-S1P antibody, LT1003. LT1007 and LT1009, with the C50A CDR mutation, exhibited binding picomolar affinities similar to LT1002.

Thermal stability may reflect stability during manufacturing and processing. Consequently, the antigen binding potency of four humanized variants was tested after incubation at various elevated temperatures (Fig. 2). The  $T_M$  for each antibody is calculated as the preincubation temperature that reduced binding potency by 50%. All humanized variants exhibited a higher  $T_M$  than that of LT1002 ( $T_M$  of 55°C), with LT1007 and LT1009 exhibiting the highest  $T_M$  values.

#### Antibody specificity for S1P over several other lipids

Table 2 shows the S1P binding specificity of LT1002 and LT1009 in competition against several other naturally oc-

curing lipids expressed as the percentage of inhibition of LT1002 binding to S1P in the presence of 2  $\mu$ M competitor. In this assay, the murine LT1002 demonstrated no cross-reactivity to SPH, the immediate metabolic precursor of S1P, or LPA, a putative extracellular signaling molecule that is structurally and functionally similar to S1P. Moreover, LT1002 did not recognize other structurally similar lipids CER, C1P, DH-S1P, PAF, PA, LPC, PA, SM, or various other phospholipids. Not shown is the lack of phosphoethanolamine binding to LT1002 shown previously (17). These findings demonstrated that the epitope recognized by the murine monoclonal antibody includes the region containing the amino alcohol on the SPH base backbone plus the free phosphate: when the free phosphate was esterified to a choline (as is the case with SPC), binding was reduced, and when the amino group was esterified to a fatty acid (as is the case with C1P), no antibody binding was observed. Furthermore, LT1002 showed no binding to LPA, which has as a glycerol backbone in-

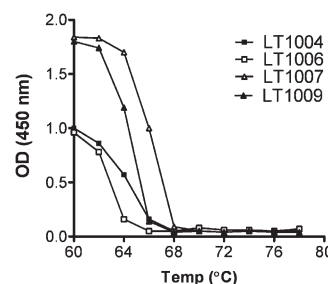


Fig. 2. Thermostability comparison of the humanized antibody variants. The thermostability of the variants was determined by measuring its S1P-binding affinity by direct binding ELISA. Each antibody (25  $\mu$ g/ml in PBS) was incubated at 60, 62, 64, 66, 68, 70, and 72, up to 78°C for 10 min and then removed insoluble material by centrifugation for 1 min at 13,000 rpm. The binding activity of the supernatant was submitted to direct S1P-binding ELISA. The  $T_M$  of the variants was determined after thermal challenge at the indicated temperature (60, 62, 64, 66, 68, 70, and 72, up to 78°C). The binding activity to S1P was then measured by ELISA and is expressed as OD at 450 nm.

stead of the SIP SPH amino alcohol backbone. Taken together, these data indicate that the epitope on SIP recognized by LT1002 is the phosphorylated amino alcohol polar head group of SIP, associated with the SPH backbone. Table 2 also indicates that LT1002 does not recognize the hydrocarbon chain in the region of the double bond of natural SIP. A detailed analysis of LT1009 binding to other SIP-related molecules in competitive ELISA confirmed that its epitope specificity was identical to that

of LT1002 (Table 2). In addition, the competitive ELISA was used to test for lack of LT1009 binding to several other lipids of varying classes, including other glycolipids, fatty acyls, glycerolipids, phospholipids, sterols, prenols, and other molecules of interest, such as FTY-720 (Table 3).

### Murine CNV model

An in vivo model of neovascularization was used to help choose which humanized antibody variant might be suit-

TABLE 3. Effects of other lipid or agents on LT1009 binding in competitive ELISA

| Common Name  | Nomenclature by Lipid Map  | Inhibition at 2 $\mu$ M (%) |
|--|--|-----------------------------|
| SIP  | Sphing-4-enine-1-phosphate   | 88.10 $\pm$ 0.32            |
| Fatty Acyls  |  |                             |
| Palmitic acid  | Hexadecanoic acid  | 0.89 $\pm$ 4.56             |
| Oleic acid   | 9Z-Octadecenoic acid   | 1.58 $\pm$ 5.28             |
| Linoleic acid  | 9Z, 12Z, 15Z-Octadecatrienoic acid   | NI                          |
| Ethyl palmitate  | Ethyl-hexadecanoate  | NI                          |
| Ethyl oleate   | Ethyl-9Z-octadecenoate   | NI                          |
| Ethyl linoleate  | Ethyl-9Z, 12Z, 15Z-octadecatrienoate   | NI                          |
| Phospholipids  |  |                             |
| Phosphatidylcholine (C16:0, 18:1)  | 1-Hexadecyl-2-(9Z-octadecyl)-sn-glycerol-3-phosphocholine  | NI                          |
| Phosphatidylglycerol (C18:2)   | 1,2-Bis-(9Z, 12Z-octadecadienoyl)-sn-3-phosphoglycerol   | 1.58 $\pm$ 5.00             |
| Phosphatidylserine (C18:0)   | 1,2-Bis-octadecyl-sn-glycero-3-phosphoserine   | 4.83 $\pm$ 1.76             |
| Phosphatidylethanolamine (C20:4)   | 1-Octadecyl-2-(5Z, 8Z, 11Z, 14Z-eicosatetraenoyl)-sn-glycero-3-phosphoethanolamine               | 4.53 $\pm$ 0.88             |
| Phosphatidylinositol (18:1)  | 1,2-Bis-(9Z-octadecadienoyl)-sn-glycero-3-phospho-(1'-myo-inositol)                              | NI                          |
| Phosphatidylinositol bisphosphate (C18:1)  | 1,2-Bis-(9Z-octadecadienoyl)-sn-glycero-3-phospho-(1'-myo-inositol-4', 5'-bisphosphate)          | NI                          |
| Phosphocholine (C16:0)   | 1-Hexadecyl-sn-glycerol-3-phosphocholine   | 1.98 $\pm$ 3.02             |
| Phosphatidic acid (C16:0-18:1)   | 1-Hexadecyl-2-(9Z-octadecenoyl)-sn-glycero-3-phosphate   | 6.29 $\pm$ 3.76             |
| Phosphatidic acid (C18:0-20:4)   | 1-Octadecyl-2-(5Z, 8Z, 11Z, 14Z-eicosatetraenoyl)-sn-glycero-3-phosphate                         | 5.66 $\pm$ 0.84             |
| Phosphatidic acid (C18:1)  | 1,2-Bis-(9Z-octadecenoyl)-sn-glycero-3-phosphate   | 0.92 $\pm$ 2.28             |
| Lysophosphatidic acid (C18:0)  | 1-Octadecyl-sn-glycerol-3-phosphate  | 4.58 $\pm$ 1.14             |
| Lysophosphatidic acid (C18:1)  | 1-(9Z-Octadecenoyl)-sn-glycerol-3-phosphate  | 7.80 $\pm$ 3.10             |
| Lysophosphatidylcholine (C18:0)  | 1-Octadecyl-sn-glycerol-3-phosphocholine   | 3.92 $\pm$ 3.36             |
| Lysophosphatidylcholine (C18:1)  | 1-(9Z-Octadecenoyl)-sn-glycerol-3-phosphocholine   | NI                          |
| Lysophosphatidylethanolamine (C18:0)   | 1-Octadecyl-sn-glycero-3-phosphoethanolamine   | NI                          |
| Lysophosphatidylglycerol (C18:0)   | 1-Octadecyl-sn-glycero-3-phosphoglycerol   | 2.50 $\pm$ 3.37             |
| Lysophosphatidylglycerol (C18:1)   | 1-(9Z-Octadecenoyl)-sn-glycero-3-phosphoglycerol   | NI                          |
| Lysophosphatidylserine (C18:1)   | 1-(9Z-Octadecenoyl)-sn-glycero-3-phosphoserine   | NI                          |
| Platelet activation factor (C16:0)   | 1-O-Hexadecyl-2-acetyl-sn-glycero-3-phosphocholine   | NI                          |
| Lyso platelet activation factor (C16:0)  | 1-O-Hexadecyl-sn-glycero-3-phosphocholine  | NI                          |
| Tetraoleoyl cardiolipin (C18:1)  | 1,3-Bis-[1,2-di-(9Z-octadecadienoyl)-sn-glycero-3-phospho]sn-glycerol                            | NI                          |
| Glycerolipids  |  |                             |
| Diacylglycerol   | 1, 2-Bis-(9Z-octadecenoyl)-sn-glycerol   | 4.81 $\pm$ 2.43             |
| Triacyl glycerol   | Tri-(9Z-octadecenoyl)-sn-glycerol  | NI                          |
| Glycosphingolipids   |  |                             |
| D-galactosyl- $\beta$ -1-1'sphingosine   | Gal $\beta$ -sphing-4-enine  | NI                          |
| Glucosyl ceramide  | Glc $\beta$ -Cer(d18:1/12:0)   | NI                          |
| Galactosyl ceramide  | Gal $\beta$ -Cer(d18:1/12:0)   | 0.44 $\pm$ 3.43             |
| Sulfatide  | (3'sulfo)Gal $\beta$ -Cer(d18:0/C24:1)   | 2.14 $\pm$ 2.28             |
| Ganglioside GMI  | Gal $\beta$ 1-3GalNAc $\beta$ 1-4(NeuAc $\alpha$ 2-3)Gal $\beta$ 1-4Glc $\beta$ -Cer(d18:1/18:0) | 0.60 $\pm$ 3.67             |
| Steroids   |  |                             |
| Cholesterol  | Cholest-5-en-3 $\beta$ -ol   | 3.90 $\pm$ 2.76             |
| Cholesteryl palmitate  | Cholest-5-en-3 $\beta$ -yl-hexadecanoate   | 5.50 $\pm$ 0.72             |
| Cholesteryl linoleate  | Cholest-5-en-3 $\beta$ -yl-e9Z, 12Z, 15Z-octadecatrienoate                                       | 7.28 $\pm$ 1.04             |
| $\beta$ -Estradiol   | 1,3,5[10]estratriene-3,17 $\beta$ -diol  | 3.44 $\pm$ 3.55             |
| Prenol lipids  |  |                             |
| Retinol Acetate  | Retinol acetate  | NI                          |
| Saccharolipids   |  |                             |
| Lipid A  | Lipid A  | NI                          |
| Polyketides  |  |                             |
| Tetracyclin  |  | NI                          |
| Others   |  |                             |
| Cyclosporin A  |  | NI                          |
| Paclitaxel   |  | NI                          |
| FTY 720  |  | NI                          |
| 2-(p-Hydroxyanilino)-4-(p-chlorophenyl) thiazole, HCl (Sphingosine kinase inhibitor) |  | NI                          |

NI, no inhibition.



able for clinical development. The human variants were tested for their abilities to inhibit CNV in parallel with LT1002 in the murine model of CNV, which involves a laser disruption of Bruch's membrane of C57Bl/6 mice (Fig. 3). In this experiment, intravitreal administration of LT1002 inhibited ocular CNV lesion formation >85% on day 14 postlaser burn. These data are in agreement with our previous work showing substantial anti-angiogenic effects of the murine mAb in the Matrigel plug assay of angiogenesis (17) and the CNV model (18). More importantly, all three of the humanized variants (LT1004, LT1007, and LT1009) inhibited neovascularization as assessed by measurement of CNV volume. In particular, LT1009 demonstrated a remarkable 98% reduction of CNV lesion volume. While all of the anti-S1P antibodies exhibited substantial and significant inhibition of the CNV lesions, the humanized and optimized variants demonstrated substantially better efficacy when compared with the parent murine antibody. The inhibition of CNV lesions by the various antibody variants were ranked as follows: LT1009 > LT1007 > LT1004 = LT1006 > LT1002. The superior efficacy of the LT1009 variant in the CNV model helped in choosing it as the lead clinical candidate.

#### In vitro release of IL-8 from SKOV3 cells is blocked by LT1002 and LT1009

The LT1002 and LT1009 mAbs were further tested for their abilities to perform in a cell-based assay. For this purpose, we chose the IL-8 release assay using a human epithelial ovarian cancer cell line, SKOV3. These tumor cells produce and release IL-8 into the cell-conditioned media after 18 h of incubation with 5  $\mu$ M S1P. Various concentrations (2–2,600  $\mu$ g/ml) of both LT1009 and LT1002 were

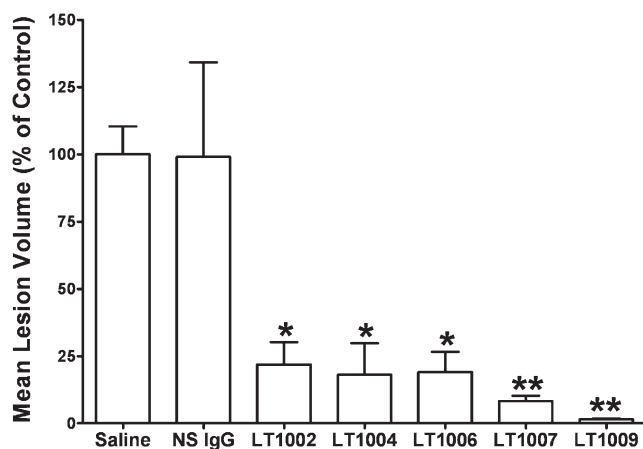


**Fig. 3.** Comparison of the in vivo efficacy of the anti-S1P mAb variants. Animals were treated with vehicle, a murine NS Ab (NS IgG), and all the anti-S1P antibodies 1 day prior to laser treatment and 6 days after laser treatment. CNV lesion volumes were measured 14 days after laser photocoagulation treatment (three burns/eye, one eye per animal, and five mice per treatment group). The areas for each burn were converted to a volume, and the volumes were averaged to produce a single CNV wound volume for each animal. All antibody treatment groups were statistically different than the saline treatment group (ANOVA followed by Bonferroni's post test: \* $P < 0.05$  and \*\* $P < 0.001$ ).

tested for their abilities to block IL-8 release in response to S1P. As shown in Fig. 4, either LT1009 or LT1002 blocked the cytokine release into the conditioned media. IC<sub>50</sub> values ( $\mu$ g/ml mAb; mean  $\pm$  SEM,  $n = 3$  independent experiments) were calculated for both LT1009 ( $374 \pm 52$ ) and LT1002 ( $513 \pm 57$ ). This suggested that LT1009 was marginally superior to LT1002 in blocking IL-8 release. IC<sub>50</sub> values are consistent with saturable bivalent binding by both LT1002 and LT1009 to S1P, which is present at 5  $\mu$ M S1P in this assay. If one assumes a molecular weight of  $\sim 150$  kDa for an antibody, then 150  $\mu$ g/ml would represent 1  $\mu$ M of full-length antibody. Further assuming that each full-length mAb has two variable regions, 150  $\mu$ g/ml antibody would represent a concentration of potential binding sites of 2  $\mu$ M. Considering that the IC<sub>50</sub> values for blockage of IL-8 release is at least double that ( $374 \mu$ g/ml for LT1009), one requires 4  $\mu$ M mAb to block 5  $\mu$ M S1P in this assay.

#### Lymphocyte trafficking pharmacodynamic study

S1P is known to play an important role in the trafficking of lymphocytes between peripheral blood and secondary lymphoid tissue (31, 32). To determine if intravenous antibody treatment would reproduce this effect, we performed a pharmacodynamic lymphocyte trafficking study in healthy mice. We also sought to compare the murine and humanize antibodies in this very sensitive in vivo experiment.

Mice received a single intravenous dose of LT1002, LT1009, control human IgG, or PBS. Total lymphocyte counts were performed on blood samples drawn prior to treatment (baseline) and 24 h after treatment. Lympho-

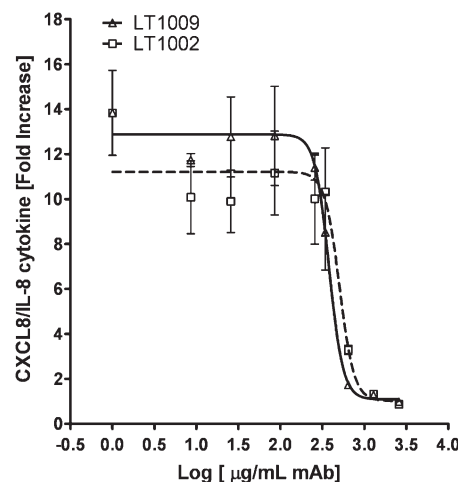


**Fig. 4.** Antibody inhibition of IL-8 release in response to S1P. Cell conditioned media from SKOV3 human ovarian cancer cells were tested for CXCL8/IL-8 levels after 18 h of incubation with 5  $\mu$ M S1P in the presence or absence of increasing concentrations of either LT1009 or LT1002 (2–2,500  $\mu$ g/ml). The addition of increasing concentrations of either LT1009 or LT1002 was able to reduce cytokine release in the cell conditioned media in a dose-dependent fashion. IC<sub>50</sub> values ( $\mu$ g/ml; mean  $\pm$  SD,  $n = 3$ ) were calculated for both LT1009 ( $374 \pm 52$ ) and LT1002 ( $513 \pm 57$ ) curves using a “nonlin fit log dose versus response” equation (GraphPad software).

cyte counts at 24 h after treatment were significantly decreased relative to pretreatment values in all animals treated with anti-S1P antibody ( $P < 0.05$ ; two-way repeated measures ANOVA with Bonferroni's correction for multiple comparisons; **Fig. 5**). The maximal decrease in lymphocyte count was to  $\sim 50\%$  of pretreatment values. Lymphocyte counts in the PBS and human IgG-treated control groups (hu-NS Ab) did not differ significantly from pretreatment values.

Based on these *in vivo* and *in vitro* data, LT1009 was declared the clinical candidate and moved forward for drug development. The *E. coli* StB12 clone containing the pATH1009 plasmid and the Chinese hamster ovary cell line LH1 275, which contain the pATH1009 plasmid, have been deposited with the ATCC (deposit numbers PTA-8421 and PTA-8422, respectively). This Chinese hamster ovary line was taken into production, and the resulting drug product is currently being used in Phase I clinical trials in cancer and AMD.

## DISCUSSION

### Anti-S1P mAbs

This work describes the production and characterization of high affinity murine (LT1002, *Sphingomab*<sup>TM</sup>) and humanized (LT1009, *Sonepcizumab*<sup>TM</sup>) mAbs specific to the bioactive lipid mediator S1P. We describe what might represent one of the first successes in producing high-affinity and specific IgG antibodies against bioactive lipids with performance characteristics suitable for a drug candidate. Moreover, we demonstrate a novel role of these antibodies as immunomodulators in their ability to affect lymphocyte trafficking.

In the past, antibodies have been produced against membrane-associated structural phospholipids, such as PS (33), phosphatidyl choline, or phospholipids associated with LDLs (28) and cardiolipin (29). However, in the case

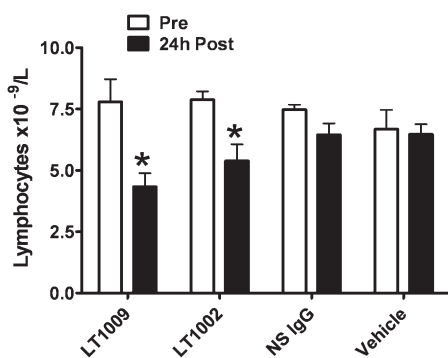


**Fig. 5.** Comparison of the ability of murine and human anti-S1P to alter lymphocyte trafficking. Peripheral blood lymphocytes were measured in mice (five/group) pre and 24 h after treatment with a single dose of antibody at 50 mg/kg. Murine (LT1002) and humanized (LT1009) anti-S1P antibodies caused a statistically significant decline in peripheral lymphocyte count when compared with pretreatment values; human nonspecific IgG (NS IgG) or PBS had no effect (two-way repeated measures ANOVA with Bonferroni's post test: \* $P < 0.05$ ).

of anti-PS antibodies, the epitope is a  $\beta 2$ -glycoprotein-PS complex (34). Moreover, anti-PS antibodies commonly recognize an oxidized rather than natural unmodified lipid (28, 29), which potentially limits their utility. In contrast, this study demonstrates that the murine and humanized anti-S1P mAbs did not recognize an oxidized state of S1P but rather were directed against the polar head group of the natural lipid. Competitive ELISA, using structurally similar bioactive lipids, mapped the epitope to the polar head group of S1P containing the *D-erythro*-oriented amino alcohol moiety of the SPH backbone plus the phosphate esterified to the terminal alcohol of the SPH base.

Monoclonal antibody generation can be envisaged as a two-part process. First, the immunogen is administered to animals in a suitable fashion so that the desired antibody response will ensue. Generating this response can be particularly difficult when the immunogen has only one unique epitope (such as the S1P polar head group) and where one could compromise epitopes when coupling the antigen to the protein carrier. Second, one must have a robust selection assay to quantitate the serological immune response and to select hybridomas. In the case of bioactive lipid small molecules, this assay is certainly as challenging as is the development of the immunogen and is an essential step required for programs designed to make mAbs against bioactive lipids.

In the first part of the method reported here, we described the conjugation of a thiolated S1P analog to the protein carrier (KLH or BSA) for immunization. We emphasize the necessity of using the thiolated S1P as part of the hapten in eliciting a robust immune response. It is critical to generate a robust immune response to the bioactive lipid without compromising the integrity of the functional epitope. We accomplished this by immunizing with the lipid covalently attached to a protein carrier via the hydrocarbon tail. This allows the antigen presentation of the unaltered polar head group.

We also believe that shortcomings in the screening assays used to detect mouse serum responders may contribute to difficulties experienced by other research groups in producing high-performance antibodies to bioactive lipids. In recognition that the screening assay would need to test the binding of antibody to the unmodified S1P-specific epitope, we elected to use thiolated S1P analog to tether S1P to a physical substrate either directly (e.g., the BiaCore chip) or indirectly via a protein carrier (e.g., for the ELISA) and then pass the antibody over the physical substrate. Assays such as these cannot only be used for antibody selection but can be used to test for specificity and other performance characteristics during humanization and during product development. These assays may also be useful as the basis of diagnostic kits for the detection of the bioactive lipid in blood and tissue.

Our competitive ELISA assay demonstrated that both LT1002 and LT1009 bind specifically S1P and do not recognize a wide variety of structurally related lipids. It was also demonstrated that LT1009 retained the same specificity as the parental LT1002 antibody. The affinities of LT1002 and LT1009 for S1P as quantified by SPR were

similar ( $K_d < 100$  pM). The affinity of both murine and humanized mAbs for SIP is 2–3 orders of magnitude higher than the affinity of SIP receptors, which is estimated to be 8–50 nM (6). One would therefore predict that the antibodies can out-compete the cognate SIP receptor GPCRs for biologically active SIP. This was confirmed both in vivo where the mAbs were capable of blocking SIP-supported angiogenesis in the mouse CNV model and in vitro where SIP-mediated release of IL-8 from ovarian cancer cells was shown to be completely mitigated. The ability of the antibody to block the IL-8 release in vitro is also consistent with our previous findings that systemic administration of LT1002 could not only reduce ovarian cancer tumor burden in mice but also decrease systemic levels of IL-8 and other pro-angiogenic cytokines in biological fluids (serum and ascites) of mice grafted with human cells secreting those cytokines (17). Thus, both murine and humanized anti-SIP antibodies can neutralize systemic or local SIP in tissues and deprive either tumor or endothelial cell GPCRs of their ligand.

We have also shown previously that systemic administration of either LT1002 or LT1009 was effective in reducing vascular endothelial growth factor and bFGF-supported angiogenesis in the in vivo Matrigel plug assay (17, 18), reduced tumor growth in murine models of human cancer (17), and that intravitreal administration of these antibodies dramatically reduced CNV lesions in vivo (18, 35). In addition, the anti-SIP mAbs have been shown to mitigate SIP-mediated actions on other cell types, such as fibroblasts (36) and macrophages (35). It is now well recognized that such cell types play an important roles not only in ocular disorders, such as AMD, but also in cancer as components of the tumor microenvironment and in other pathologies associated with impaired wound healing, scar formation, pathological ocular, and immune responses (13).

The role of SIP in the regulation of lymphocyte trafficking has been studied extensively, although the exact mechanism of action remains controversial (reviewed in Ref. 37). The SIP analog FTY-720 is a functional antagonist of SIP activity as it binds to and downregulates expression of SIP receptors (38). These results in a transient, ~40% decrease in peripheral blood lymphocyte counts (39). In this report, we have also shown that treatment of mice with anti-SIP mAbs transiently depletes peripheral blood lymphocytes in a fashion similar to that observed with FTY-720. Small molecule antagonists of SIP receptors, such as FTY-720, cause the retention of recirculating lymphocytes within the secondary lymphoid organs, resulting in a transient loss of these cells from the peripheral blood, and it has been proposed that this phenomenon can be used as a pharmacodynamic marker for development of drugs targeting the SIP axis (40).


### Therapeutic potential of LT1009

Using the CNV model of angiogenesis, we demonstrated in this report that the humanized variants could block neovascularization triggered by SIP in murine ocular lesions. This model helped to identify the humanized lead

compound, LT1009, to be brought forward into clinical trials for treatment of AMD as well as cancer. In addition to the inhibitory effects of LT1009 on SIP-dependent cancer cell growth and endothelial cell function, the anti-SIP mAbs have been shown to mitigate SIP-mediated actions on other cell types such as fibroblasts (36) and macrophages (35). It is now well recognized that such cell types play important roles not only in ocular disorders, such as AMD, but also in cancer as components of the tumor microenvironment and also in other pathologies associated with impaired wound healing, scar formation, pathological ocular angiogenesis, and immune responses (13). Sutphen et al. (41) have shown that serum SIP levels are elevated in early- and late-stage ovarian cancer patients. Importantly, SPHK1, the enzyme that is responsible for the production of SIP, is found significantly upregulated in a variety of cancer types (10, 11) and that disease progression can be correlated with SPHK1 overexpression (12). In addition, SPHK1 activity has been shown in several cancer cell lineages to be responsible for resistance to cytotoxics (42–45). Thus, we speculate that LT1009 might improve the potency of chemotherapeutic drugs by improving patient sensitivity to the agent. We also speculate that LT1009 could be used as a therapeutic “molecular sponge” to selectively absorb SIP produced by any condition characterized by the upregulated activity of SPHK1 and resulting SIP production. Accordingly, LT1009 is now being tested for safety and maximum tolerated dose in clinical trials for cancer and AMD.

Considering the abundant levels of SIP in human plasma (~0.5  $\mu$ M) (46), one may be concerned about the side effects of neutralizing all of the SIP in the periphery, particularly since this level of SIP far exceeds the  $K_d$  for SIP receptors (8–50 nM). If it were the case that a substantial amount of plasma SIP was available to receptors, one could predict that the neutralization of SIP with mAbs might have toxicological and/or expected pharmacological effects. Importantly, pivotal 28-day Good Laboratory Practice toxicology studies in nonhuman primates (NHPs) showed that LT1009 was well tolerated with substantial dose exposure (up to 100 mg/kg, q3d) including the absence of toxicity or pathological changes (data not shown). SIP is known to be anti-apoptotic in cell culture. Apparently, this protective effect is likely not a role for SIP in the peripheral circulation, and it may only occur in the microenvironment of tumors or tissues engaged in beneficial inflammatory or wound healing responses. It is likely the serum proteins like albumin, HDLs, and LDLs act as buffers for SIP to ensure that the biologically active fraction of SIP is below that of SIP receptors (47). The major finding in the nonpivotal mouse and pivotal NHP toxicology studies was an effect on lymphocyte levels similar to the data reported here. The Phase 1 clinical trial for ASONEP (the oncology formulation of sonenpcizumab, LT1009) is nearing completion, and the Phase 2 efficacy studies are being planned. Assuming that sonenpcizumab demonstrates that it is as well tolerated in humans as it is in NHPs and mice, the planned clinical studies will determine its therapeutic index and clinical efficacy.



The nomenclature of the following lipids used in this study was based on the LIPID MAP INITIATIVE: sphingosine-1-phosphate, sphing-4-enine-1-phosphate; palmitic acid, hexadecanoic acid; oleic acid, 9Z-octadecenoic acid; linoleic acid, 9Z, 12Z, 15Z-octadecatrienoic acid; ethyl palmitate; ethyl oleate, ethyl-hexadecanoate; ethyl linoleate, ethyl-9Z-octadecenoate, ethyl-9Z, 12Z, 15Z-octadecatrienoate; diacylglycerol (C18:1), 1, 2-bis-(9Z-octadecenoyl)-sn-glycerol; triacylglycerol (C18:1), tri-(9Z-octadecenoyl)-sn-glycerol, phosphatidylcholine (C16:0, C18:1), 1-hexadecyl-2-(9Z-octadecyl)-sn-glycerol-3-phosphocholine; phosphatidylglycerol (C18:2), 1,2-bis-(9Z, 12Z-octadecadienoyl)-sn-3-phosphoglycerol; phosphatidylserine (C18:0), 1,2-bis-octadecyl-sn-glycero-3-phosphoserine; phosphatidylethanolamine (C20:4), 1-octadecyl-2-(5Z, 8Z, 11Z, 14Z-eicosatetraenoyl)-sn-glycero-3-phosphoethanolamine; phosphatidylinositol (C18:1), 1,2-bis-(9Z-octadecadienoyl)-sn-glycero-3-phospho-(1'-myo-inositol); phosphatidylinositol bisphosphate (C18:1), 1,2-bis-(9Z-octadecadienoyl)-sn-glycero-3-phospho-(1'-myo-inositol-4', 5'-bisphosphate); phosphocholine (C16:0), 1-hexadecyl-sn-glycerol-3-phosphocholine; phosphatidic acid (C16:0-18:1), 1-hexadecyl-2-(9Z-octadecenoyl)-sn-glycero-3-phosphate; phosphatidic acid (C18:0-20:4), 1-octadecyl-2-(5Z, 8Z, 11Z, 14Z-eicosatetraenoyl)-sn-glycero-3-phosphate; phosphatidic acid (C18:1), 1, 2-bis-(9Z-octadecenoyl)-sn-glycero-3-phosphate; lysophosphatidic acid (C18:0), 1-octadecyl-sn-glycerol-3-phosphate; lysophosphatidic acid (C18:1), 1-(9Z-octadecenoyl)-sn-glycerol-3-phosphate; lysophosphatidylcholine (C18:0), 1-octadecyl-sn-glycerol-3-phospholine; lysophosphatidylcholine (C18:1), 1-(9Z-octadecenoyl)-sn-glycerol-3-phosphocholine; lysophosphatidylethanolamine (C18:0), 1-octadecyl-sn-glycero-3-phosphoethanolamine; lysophosphatidylglycerol (C18:0), 1-octadecyl-sn-glycero-3-phosphoglycerol; lysophosphatidylglycerol (C18:1), 1-(9Z-octadecenoyl)-sn-glycero-3-phosphoglycerol; lysophosphatidylserine (C18:1), 1-(9Z-octadecanoyl)-sn-glycero-3-phosphoserine; platelet activation factor (C16:0), 1-O-hexadecyl-2-acetyl-sn-glycero-3-phosphocholine; lyso platelet activation factor (C16:0), 1-O-hexadecyl-sn-glycero-3-phosphocholine; tetraoleoyl cardiolipin (C18:1), 1,3-bis-[1,2-di-(9Z-octadecadienoyl)-sn-glycero-3-phospho]-sn-glycerol; D-galactosyl- $\beta$ -1-1' sphingosine, Gal $\beta$ -sphing-4-enine; glucosyl ceramide, Glc $\beta$ -Cer(d18:1/12:0); galactosylceramide, Gal $\beta$ -Cer(d18:1/12:0); sulfatide, (3'sulfo)Gal $\beta$ -Cer(d18:0/C24:1); ganglioside GM1, Gal $\beta$ 1-3GalNAc $\beta$ 1-4(NeuAc $\alpha$ 2-3)Gal $\beta$ 1-4Glc $\beta$ -Cer(d18:1/18:0); cholesterol, cholest-5-en-3 $\beta$ -ol; cholesteryl palmitate, cholest-5-en-3 $\beta$ -yl-hexadecanoate; cholesteryl linoleate, cholest-5-en-3 $\beta$ -yl-e9Z, 12Z, 15Z-octadecatrienoate;  $\beta$ -estradiol, 1,3,5[10]estratriene-3,17 $\beta$ -diol. Lpath is willing to share the murine mAb with qualified investigators under an agreeable materials transfer agreement. 

The authors acknowledge the help of William Garland and Manoj Sharma in the planning of many of the studies reported here.

- Gardell, S. E., A. E. Dubin, and J. Chun. 2006. Emerging medicinal roles for lysophospholipid signaling. *Trends Mol. Med.* **12**: 65–75.
- Murph, M., and G. B. Mills. 2007. Targeting the lipids LPA and S1P and their signalling pathways to inhibit tumour progression. *Expert Rev. Mol. Med.* **9**: 1–18.
- Skoura, A., T. Sanchez, K. Claffey, S. M. Mandala, R. L. Proia, and T. Hla. 2007. Essential role of sphingosine 1-phosphate receptor 2 in pathological angiogenesis of the mouse retina. *J. Clin. Invest.* **117**: 2506–2516.
- Wymann, M. P., and R. Schneider. 2008. Lipid signalling in disease. *Nat. Rev. Mol. Cell Biol.* **9**: 162–176.
- Milstien, S., and S. Spiegel. 2006. Targeting sphingosine-1-phosphate: a novel avenue for cancer therapeutics. *Cancer Cell.* **9**: 148–150.
- Chun, J., and H. Rosen. 2006. Lysophospholipid receptors as potential drug targets in tissue transplantation and autoimmune diseases. *Curr. Pharm. Des.* **12**: 161–171.
- Cuvillier, O., G. Pirianov, B. Kleuser, P. G. Vanek, O. A. Coso, S. Gutkind, and S. Spiegel. 1996. Suppression of ceramide-mediated programmed cell death by sphingosine-1-phosphate. *Nature.* **381**: 800–803.
- Pyne, S., and N. J. Pyne. 2000. Sphingosine 1-phosphate signalling in mammalian cells. *Biochem. J.* **349**: 385–402.
- Baran, Y., A. Salas, C. E. Senkal, U. Gunduz, J. Bielawski, L. M. Obeid, and B. Ogretmen. 2007. Alterations of ceramide/sphingosine 1-phosphate rheostat involved in the regulation of resistance to imatinib-induced apoptosis in K562 human chronic myeloid leukemia cells. *J. Biol. Chem.* **282**: 10922–10934.
- French, K. J., R. S. Schrecengost, B. D. Lee, Y. Zhuang, S. N. Smith, J. L. Eberly, J. K. Yun, and C. D. Smith. 2003. Discovery and evaluation of inhibitors of human sphingosine kinase. *Cancer Res.* **63**: 5962–5969.
- Johnson, K. R., K. Y. Johnson, H. G. Crellin, B. Ogretmen, A. M. Boylan, R. A. Harley, and L. M. Obeid. 2005. Immunohistochemical distribution of sphingosine kinase 1 in normal and tumor lung tissue. *J. Histochem. Cytochem.* **53**: 1159–1166.
- Van Brocklyn, J. R., C. A. Jackson, D. K. Pearl, M. S. Kotur, P. J. Snyder, and T. W. Prior. 2005. Sphingosine kinase-1 expression correlates with poor survival of patients with glioblastoma multiforme: roles of sphingosine kinase isoforms in growth of glioblastoma cell lines. *J. Neuropathol. Exp. Neurol.* **64**: 695–705.
- Sabbadini, R. A. 2006. Targeting sphingosine-1-phosphate for cancer therapy. *Br. J. Cancer.* **95**: 1131–1135.
- Vadas, M., P. Xia, G. McCaughan, and J. Gamble. 2008. The role of sphingosine kinase 1 in cancer: Oncogene or non-oncogene addiction? *Biochim. Biophys. Acta.* **1781**: 442–447.
- Baumruker, T., A. Billich, and V. Brinkmann. 2007. FTY720, an immunomodulatory sphingolipid mimetic: translation of a novel mechanism into clinical benefit in multiple sclerosis. *Expert Opin. Investig. Drugs.* **16**: 283–289.
- Kappos, L., J. Antel, G. Comi, X. Montalban, P. O'Connor, C. H. Polman, T. Haas, A. A. Korn, G. Karlsson, and E. W. Radue. 2006. Oral fingolimod (FTY720) for relapsing multiple sclerosis. *N. Engl. J. Med.* **355**: 1124–1140.
- Visentin, B., J. A. Vekich, B. J. Sibbald, A. L. Cavalli, K. M. Moreno, R. G. Matteo, W. A. Garland, Y. Lu, S. Yu, H. S. Hall, et al. 2006. Validation of an anti-sphingosine-1-phosphate antibody as a potential therapeutic in reducing growth, invasion, and angiogenesis in multiple tumor lineages. *Cancer Cell.* **9**: 225–238.
- Caballero, S., J. Swaney, K. Moreno, A. Afzal, J. Kielczewski, G. Stoller, A. Cavalli, W. Garland, G. Hansen, R. Sabbadini, et al. 2009. Anti-sphingosine-1-phosphate monoclonal antibodies inhibit angiogenesis and sub-retinal fibrosis in a murine model of laser-induced choroidal neovascularization. *Exp. Eye Res.* **88**: 367–377.
- Winter, G. P. 1989. Antibody engineering. *Philos. Trans. R. Soc. Lond. B Biol. Sci.* **324**: 537–546 (discussion 547).
- Morea, V., A. M. Lesk, and A. Tramontano. 2000. Antibody modeling: implications for engineering and design. *Methods.* **20**: 267–279.
- Kabat, E. A., T. T. Wu, H. M. Perry, K. S. Gottsman, and C. Foeller. 1991. Sequences of proteins of immunological interest. Public Health Service. 5th ed. National Institutes of Health, Bethesda, MD.
- Chothia, C., J. Novotny, R. Brucoleri, and M. Karplus. 1985. Domain association in immunoglobulin molecules. The packing of variable domains. *J. Mol. Biol.* **186**: 651–663.

23. Foote, J., and G. Winter. 1992. Antibody framework residues affecting the conformation of the hypervariable loops. *J. Mol. Biol.* **224**: 487–499.
24. Sengupta, N., S. Caballero, R. N. Mames, A. M. Timmers, D. Saban, and M. B. Grant. 2005. Preventing stem cell incorporation into choroidal neovascularization by targeting homing and attachment factors. *Invest. Ophthalmol. Vis. Sci.* **46**: 343–348.
25. Sengupta, N., S. Caballero, R. N. Mames, J. M. Butler, E. W. Scott, and M. B. Grant. 2003. The role of adult bone marrow-derived stem cells in choroidal neovascularization. *Invest. Ophthalmol. Vis. Sci.* **44**: 4908–4913.
26. Vielhaber, G., L. Brade, B. Lindner, S. Pfeiffer, R. Wepf, U. Hintze, K. P. Wittern, and H. Brade. 2001. Mouse anti-ceramide antiserum: a specific tool for the detection of endogenous ceramide. *Glycobiology.* **11**: 451–457.
27. Krishnamurthy, K., S. Dasgupta, and E. Bieberich. 2007. Development and characterization of a novel anti-ceramide antibody. *J. Lipid Res.* **48**: 968–975.
28. Chang, M. K., C. Bergmark, A. Laurila, S. Horkko, K. H. Han, P. Friedman, E. A. Dennis, and J. L. Witztum. 1999. Monoclonal antibodies against oxidized low-density lipoprotein bind to apoptotic cells and inhibit their phagocytosis by elicited macrophages: evidence that oxidation-specific epitopes mediate macrophage recognition. *Proc. Natl. Acad. Sci. USA.* **96**: 6353–6358.
29. Horkko, S., E. Miller, E. Dudl, P. Reaven, L. Curtiss, N. Zvaifler, R. Terkeltaub, S. Pierangeli, D. Branch, W. Palinski, et al. 1996. Antiphospholipid antibodies are directed against epitopes of oxidized phospholipids: recognition of cardiolipid by monoclonal antibodies to epitopes of oxidized low density lipoprotein. *J. Clin. Invest.* **98**: 815–825.
30. Deutschman, D. H., J. S. Carstens, R. I. Klepper, W. S. Smith, M. T. Page, T. R. Young, L. A. Gleason, N. Nakajima, and R. A. Sabbadini. 2003. Predicting obstructive coronary artery disease using serum sphingosine-1-phosphate. *Am. Heart J.* **146**: 62–68.
- 30a. Wojciak, J., N. Zhu, K. Schuereberg, K. Moreno, W. Shestowksy, M. Hiraiwa, R. Sabbadini, and T. Huxford. The crystal structure of sphingosine-1-phosphate in complex with a Fab fragment reveals metal bridging of an antibody and its antigen. *Proc. Natl. Acad. Sci.* Sept 28, 2009. [Epub ahead of print].
31. Matloubian, M., C. G. Lo, G. Cinamon, M. J. Lesneski, Y. Xu, V. Brinkmann, M. L. Allende, R. L. Proia, and J. G. Cyster. 2004. Lymphocyte egress from thymus and peripheral lymphoid organs is dependent on SIP receptor 1. *Nature.* **427**: 355–360.
32. Brinkmann, V., J. G. Cyster, T. Hla, S. S. Chae, R. L. Proia, J. D. Saba, H. Ozaki, M. J. Lee, T. Sanchez, T. Estrada-Hernandez, et al. 2004. FTY720: sphingosine 1-phosphate receptor-1 in the control of lymphocyte egress and endothelial barrier function. *Am. J. Transplant.* **4**: 1019–1025.
33. Diaz, C., K. Balasubramanian, and A. J. Schroit. 1998. Synthesis of disulfide-containing phospholipid analogs for the preparation of head group-specific lipid antigens: generation of phosphatidylserine antibodies. *Bioconjug. Chem.* **9**: 250–254.
34. Luster, T. A., J. He, X. Huang, S. N. Maiti, A. J. Schroit, P. G. de Groot, and P. E. Thorpe. 2006. Plasma protein beta-2-glycoprotein 1 mediates interaction between the anti-tumor monoclonal antibody 3G4 and anionic phospholipids on endothelial cells. *J. Biol. Chem.* **281**: 29863–29871.
35. Xie, B., J. Shen, A. Dong, A. Rashid, G. Stoller, and P. A. Campochiaro. 2009. Blockade of sphingosine-1-phosphate reduces macrophage influx and retinal and choroidal neovascularization. *J. Cell. Physiol.* **218**: 192–198.
36. Swaney, J. S., K. M. Moreno, A. M. Gentile, R. A. Sabbadini, and G. L. Stoller. 2008. Sphingosine-1-phosphate (S1P) is a novel fibrotic mediator in the eye. *Exp. Eye Res.* **87**: 367–375.
37. Brinkmann, V. 2007. Sphingosine 1-phosphate receptors in health and disease: mechanistic insights from gene deletion studies and reverse pharmacology. *Pharmacol. Ther.* **115**: 84–105.
38. Graler, M. H., and E. J. Goetzl. 2004. The immunosuppressant FTY720 down-regulates sphingosine 1-phosphate G-protein-coupled receptors. *FASEB J.* **18**: 551–553.
39. Kovarik, J. M., R. L. Schmouder, and A. J. Slade. 2004. Overview of FTY720 clinical pharmacokinetics and pharmacology. *Ther. Drug Monit.* **26**: 585–587.
40. Rohatagi, S., H. Zahir, J. B. Moberly, K. E. Truitt, S. Inaba, T. Shimozato, and T. J. Carrothers. 2009. Use of an exposure-response model to aid early drug development of an oral sphingosine 1-phosphate receptor modulator. *J. Clin. Pharmacol.* **49**: 50–62.
41. Sutphen, R., X. Y. Wilbanks, G. D. Fiorica, J. Grendys, E. C. Jr, J. P. LaPolla, H. Arango, M. S. Hoffman, M. Martino, K. Wakeley, et al. 2004. Lysophospholipids are potential biomarkers of ovarian cancer. *Cancer Epidemiol. Biomarkers Prev.* **13**: 1185–1191.
42. Anelli, V., C. R. Gault, A. B. Cheng, and L. M. Obeid. 2008. Sphingosine kinase 1 is up-regulated during hypoxia in U87MG glioma cells. Role of hypoxia-inducible factors 1 and 2. *J. Biol. Chem.* **283**: 3365–3375.
43. Bonhoure, E., A. Lauret, D. J. Barnes, C. Martin, B. Malavaud, T. Kohama, J. V. Melo, and O. Cuvillier. 2008. Sphingosine kinase-1 is a downstream regulator of imatinib-induced apoptosis in chronic myeloid leukemia cells. *Leukemia.* **22**: 971–979.
44. Sarkar, S., M. Maceyka, N. C. Hait, S. W. Paugh, H. Sankala, S. Milstien, and S. Spiegel. 2005. Sphingosine kinase 1 is required for migration, proliferation and survival of MCF-7 human breast cancer cells. *FEBS Lett.* **579**: 5313–5317.
45. Pchejetski, D., M. Golzio, E. Bonhoure, C. Calvet, N. Doumerc, V. Garcia, C. Mazerolles, P. Rischmann, J. Teissie, B. Malavaud, et al. 2005. Sphingosine kinase-1 as a chemotherapy sensor in prostate adenocarcinoma cell and mouse models. *Cancer Res.* **65**: 11667–11675.
46. Scherer, M., G. Schmitz, and G. Liebisch. 2009. High-throughput analysis of sphingosine 1-phosphate, sphinganine 1-phosphate, and lysophosphatidic acid in plasma samples by liquid chromatography-tandem mass spectrometry. *Clin Chem.* **55**: 1218–1222.
47. Murata, N., K. Sato, J. Kon, H. Tomura, and F. Okajima. 2000. Quantitative measurement of sphingosine 1-phosphate by radio-receptor-binding assay. *Anal. Biochem.* **282**: 115–120.

## ERRATA

The authors of "Label-free quantitative analysis of lipid metabolism in living *Caenorhabditis elegans*" (*J. Lipid Res.* 51: 672–677) have advised the *Journal* that the figure legend for Figure 2 of their manuscript is incorrect. It should read as follows:

**Fig. 2.** Expression levels of lipid species in the wild type and mutant *C. elegans*. A: CARS imaging of lipid (red) and TPEF imaging of autofluorescent lipid species (blue) of adult N2 wild-type and mutant *C. elegans*. Images are presented as three-dimensional projections of 36 frames taken along the vertical axis at 1  $\mu\text{m}$  intervals. Expression levels of neutral lipid droplets (B) and autofluorescent lipid droplets (C) as a function of wild-type and mutant worms. Expression levels are normalized to 1 for the wild type and comparatively for mutants. Error bars represent distribution across six adult wild-type or mutant *C. elegans*. D: Biochemical measurements of cholesterol level and superoxide dismutase (SOD) activity. Expression levels are normalized to 1 for the wild type and comparatively for mutant *C. elegans*. Error bars represent distribution across three repeated experiments.

The incorrect figure legend initially appeared online but has since been corrected.

---

DOI 10.1194/jlr.D000638ERR

The authors of "Production and characterization of monoclonal anti-sphingosine-1-phosphate antibodies" (*J. Lipid Res.* 50: 2245–2257) have advised the *Journal* that the name of an oligo stated in the Materials and Methods section of their manuscript is incorrect. The mouse immunoglobulin kappa chain variable region (VL) was amplified by PCR using **VK20**, not MKV20.

This incorrect oligo name initially appeared online but has since been corrected.

---

DOI 10.1194/jlr.M900048ERR